Journal of Science: Advanced Materials and Devices 9 (2024) 100716

Contents lists available at ScienceDirect

Journal of Science: Advanced Materials and Devices

journal homepage: www.elsevier.com/locate/jsamd

Expanding the applications of the wear-resistant titanium aluminum nitride thin-film to include temperature sensing

Bruno Martins [a,b,*], Carlos Patacas [a,b], Albano Cavaleiro [a,b], Pedro Faia [c], Fátima Zorro [e,f], Enrique Carbo-Argibay [e], Paulo J. Ferreira [e,f,g], Filipe Fernandes [b,d]

[a] IPN - LED&MAT - Instituto Pedro Nunes, Laboratório de Ensaios, Desgaste e Materiais, Rua Pedro Nunes, 3030-199, Coimbra, Portugal
[b] University of Coimbra, CEMMPRE, ARISE, Department of Mechanical Engineering, Rua Luís Reis Santos, 3030-788, Coimbra, Portugal
[c] University of Coimbra, CEMMPRE – Electrical and Computer Engineering Department, FCTUC, Polo 2, Pinhal de Marrocos, Coimbra, 3030-290, Portugal
[d] CIDEM, ISEP - Polytechnic of Porto, Rua Dr. António Bernardino de Almeida, 4249-015, Porto, Portugal
[e] International Iberian Nanotechnology Laboratory (INL), Avenida Mestre Jose Veiga, 4715-330, Braga, Portugal
[f] Mechanical Engineering Department and IDMEC, Instituto Superior Técnico, Av. Rovisco Pais 1, 1049-001, Lisboa, Portugal
[g] Materials Science and Engineering Program, University of Texas at Austin, Austin, TX, 78712, USA

ARTICLE INFO

Keywords:
NTC thin-film thermistor
Magnetron sputtering
Nitride semiconductors
Multilayer coating
Temperature sensing

ABSTRACT

This study investigates an approach to temperature sensing by integrating Titanium Aluminum Nitride (TiAlN), originally engineered for wear and corrosion applications, as a temperature sensor within a multilayered thin film system. A nitride multilayer system was developed by physical vapor deposition (PVD) using a single four-target magnetron sputtering chamber; intermediate vacuum interruption steps were employed for masking procedures. The multilayer architecture design aimed to provide the sensor layer with mechanical protection and electrical shielding. Structural and electrical characterization of the TiAlN single layer revealed semiconductor behavior and stable electrical resistance up to 750 °C, with minimal signal stabilization requirements. Despite the higher Al content, the TiAlN temperature sensor exhibited a cubic crystal structure characterized by diffuse nanolayers, resulting from a two-fold rotational deposition and target configuration. A detailed examination of the multilayer system cross-section containing the TiAlN sensor was conducted using scanning transmission electron microscopy (STEM). The analysis revealed its columnar morphology with the presence of typical PVD growth defects, including voids and droplets. While the presence of these defects may impact the electrical characteristics of the sensor, the selected experimental conditions effectively maintained the structural integrity of the multilayer system despite the vacuum interruptions caused by masking procedures. Validation experiments confirmed the functionality of the multilayer system for temperature measurements up to 400 °C. The signal acquisition system addressed room temperature resistance variations and low sensitivity (thermistor coefficient ~100 K), resulting in a measured error of approximately 6%. This study demonstrates promising results of TiAlN as a temperature sensor within a multilayered system, expanding its range of potential applications.

1. Introduction

Temperature is a critical variable in manufacturing processes that profoundly impacts operations in various industrial sectors [1]. As the manufacturing industry landscape advances to meet the demands of Industry 4.0, where data-driven strategies are vital for enhancing operational efficiency, the importance of temperature dynamics becomes even more evident. Thin films have long been recognized in the manufacturing industry for their role in tooling protection in high-temperature and abrasive conditions [2,3]. These protective thin films are usually positioned where a deep understanding of process dynamics, including temperature or pressure, is indispensable [4,5]; therefore, materials with protective and electrical properties would be essential for the industry to translate pivotal variables such as temperature in real time. Consequently, there has been a persistent interest in developing physical vapor deposition (PVD) wear-resistant coatings incorporating sensing functionalities. These integrated sensor coatings are active in providing electrical signals for critical manufacturing

Peer review under responsibility of Vietnam National University, Hanoi.
* Corresponding author. IPN - LED&MAT - Instituto Pedro Nunes, Laboratório de Ensaios, Desgaste e Materiais, Rua Pedro Nunes, 3030-199 Coimbra, Portugal.
E-mail address: brunomartins@ipn.pt (B. Martins).

https://doi.org/10.1016/j.jsamd.2024.100716
Received 14 February 2024; Received in revised form 28 March 2024; Accepted 4 April 2024
Available online 9 April 2024

processes, such as injection molding [6] or forming [7] and machining [8].

A multilayer architecture design is essential for developing sensor coatings for temperature measurement since the sensor layer must be electrically isolated from the surroundings. In addition, the inclusion of a top wear resistance layer is applied to protect the underlying layers. Therefore, numerous studies in the literature for industrial applications, for example, from injection molding [6,9] to metal cutting [8,10,11], follow the multilayer approach. In one of the used approaches, the temperature sensor was encapsulated between hydrogenated carbon and carbon modified with silicon and oxygen films [6,7]. The C:Si:O outer layer served for insulating and wear protection purposes, reducing the number of layers in the coating. However, the 8 GPa of hardness acknowledged for this layer can compromise the wear performance of the coating, which was not explored in the work. In addition, the multilayer architecture was accomplished by combining plasma-enhanced chemical vapor deposition (PECVD) and PVD, which increases the complexity of developing these coatings. The utilization of different thin film technologies is the path that most researchers follow. Li et al. [8], developed a sensor coating by employing thermal evaporation, sputtering, and diffusion bonding techniques. In other reports dealing with the measurement of temperature in machining applications, PECVD and PVD were used to deposit a sensor coating with thin film thermocouples (TFTC) in the cutting tools [10,11]. To measure the temperature in engine turbine blades [4], a coating sensor with a thermocouple was developed by screen printing in combination with pulse laser deposition. Only a few studies in literature simplify the process by using only one thin film technique. For instance, Bobzin et al. [5], developed a multilayer system with a TFTC based on the sputtering technique for temperature measurement in general applications. However, the authors did not test their system with an insulative top film to protect the sensor, and the effect of depositing an additional layer in the microstructure and electrical properties of the sensor is unknown. In addition for using diverse deposition methods, the predominant use of photolithography for patterning the sensor layer adds further intricacy and cost to the multilayer coating design [6–9].

According to Niu et al. [4], the thermocouple is the predominant method for measuring surface temperature, supported by the few studies addressing the thermoresistive method [6,7,9]. In some approaches, temperature is determined by measuring the linear dependence of electrical resistance with temperature in chromium, resulting in a positive temperature coefficient of resistance (PTCR) [6,7]. Oliveira and colleagues [9], used the same temperature measurement method. Though the resistance decreases non-linearly with temperature, as a sensor thermistor based on semiconductor possessing a negative temperature coefficient of resistance (NTCR). Thermocouples are also popular sensors due to their wide range of temperatures, reasonable linearity, and fast response time [12]. However, TFTC requires two dissimilar layers to promote the thermoelectric effect [4,5,8,10,11], which means additional interfaces or weak spots. In addition, these sensors must have cold-junction compensation and precision amplification due to low output signals [12], and the calibration procedures for the TFTC with cold-junction are often absent in the studies [5,8]. In contrast, resistive sensors, like an NTCR thermistor, do not need compensation, and signal acquisition can be accomplished by a simple voltage divider [12]. Thin film thermistors can be deposited in one step instead of the two steps required for TFTC [9], but due to their high sensitivities and non-linearity, the range of temperature is limited. This can be the main reason for the missing of studies on the application of sensor coatings using thermistors in manufacturing applications [13]. To overcome this limitation, recent studies have been conducted on the electrical properties of the titanium aluminum nitride (TiAlN) [14,15], state-of-the-art PVD coating for cutting tools, to understand their behavior as thermistor sensors. TiAlN films with specific chemical compositions display semiconductor behavior and can have thermistor functionality [15]. Overall, temperature acquisition through sensor coatings is established; however, there still are limitations which are delaying the scale-up of those sensors from laboratory environment to industrial applications. Specifically, there is a critical need to address the practical challenges associated with the interfaces within these multilayer coatings, such as the complexity introduced by using multiple deposition techniques and the dependence on photolithography for patterning. In addition, a notable gap in the literature is found regarding integrating three distinct layers in sensor coatings, each serving different functions, including insulation, sensing, and wear resistance.

To address the limitations above, this study focuses on the deposition of a TiAlN thermistor sensor integrated within a multilayer system, including aluminum nitride (AlN) acting as an insulator layer and another of TiAlN used as a wear-resistant layer. All the layers were deposited by magnetron sputtering, resulting in a fully nitride sensor coating. The thermistor layer was developed based on previous work reported by the current authors [15], and its functionality as a sensor was tested up to 750 °C. The sensor patterning was accomplished using Kapton® tape, which is traced accordingly by means of a UV laser cutting equipment. The interfaces between the sensor and the adjacent layers were thoroughly analyzed, as this was the most critical step due to the patterning process. Considering the significance of temperature in cutting applications, the multilayer coating was deployed in a conventional cutting tool substrate and used for calibrating the system – sensor coating including acquisition system – against a reference thermocouple up to 400 °C. However, it is our understanding that this sensor coating architecture can be applied in various components working under high-temperature solicitations. To demonstrate the seamless integration of this system into the context of Industry 4.0, an Arduino® board equipped with Wi-Fi and Bluetooth® connectivity was used as a signal acquisition system.

2. Experimental

2.1. Sensor deposition and patterning strategy

The sensor coating composed of four films – AlN (insulator) + TiAlN (sensor) + AlN (insulator) + TiAlN (wear resistance) – was deposited using a PVD equipment equipped with four targets in a closed-field magnetic configuration, using two titanium and two aluminum targets, as shown in Fig. 1. This layering design was planned to ensure proper electrical insulation and wear protection. According to the previous study of the current authors [15], it is possible to attain a TiAlN temperature sensor with a cubic crystal structure within adequate chemical composition. The wear-resistant layer's TiAlN was deposited using the same sputtering parameters employed for the TiAlN sensor, starting with AlN and subsequently transitioning to TiAlN through a gradual increase in the power density of the Ti targets. A thin Ti adhesion layer was intentionally introduced to enhance the final layer's adhesion to the multilayer system. A mixture of argon and nitrogen (the reactive gas) was used to allow the formation of the desired compounds. The principal deposition conditions for the AlN and TiAlN are presented in Table 1. It is important to note that the comprehensive characterization of the AlN compound is beyond the scope of this study and will be presented in a separate work. The sensor coating procedure involved five steps: (1) deposition of the AlN layer in a conventional cutting tool substrate; (2) patterning of the TiAlN sensor; (3) masking and deposition of the second AlN layer; (4) deposition of the TiAlN wear-resistant layer according to the mask design; (5) masking and deposition of TiN contacts for signal acquisition. A meander design was considered for the sensor to achieve the desired room temperature resistance (R25) within 10 kΩ range. To pattern the sensor, Kapton® tape was utilized as a shadow mask and tailored using a UV laser equipment. Initially, the tape was laser-cut in accordance with the sensor design, and by removing any residual adhesive within the traces to ensure a clear path for the coating. Finally, the Kapton® mask was placed in the substrate using transfer tape with a magnifier to ensure precise positioning. The masking

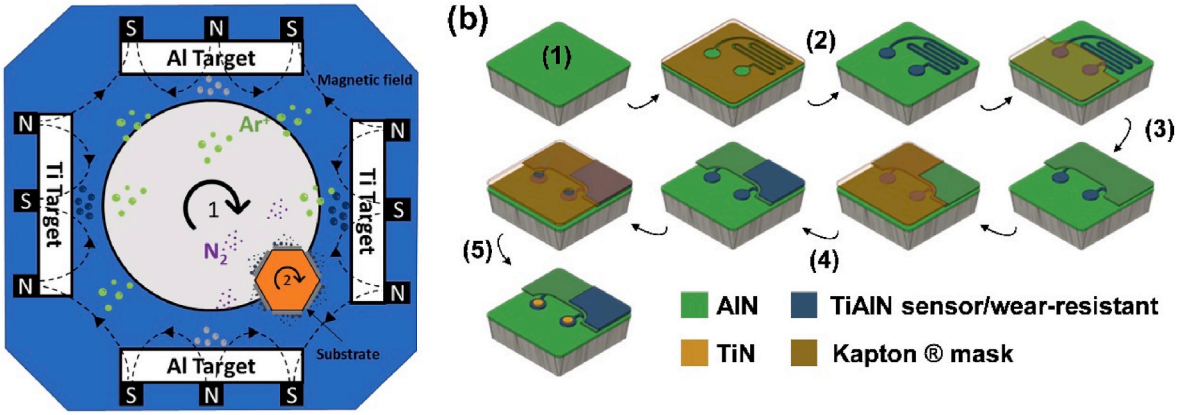

Fig. 1. (a) Target configuration for the deposition of the multilayer system; (b) Masking procedure to deposit the sensor coating in a cutting tool.

Table 1
The main deposition parameters used to produce the single TiAlN temperature sensor and the multilayer coating.

	TiAlN/Sensor/Wear	AlN	TiN
Ultimate vacuum (Pa)	$<5x10^{-4}$	$<5x10^{-4}$	$<5x10^{-4}$
Substrates in-situ cleaning – physical etching			
Substrate bias (V)	−300	−650	−300
Time (min)	15	60	15
Ar pressure (Pa)	0.1	0.1	0.1
Targets power density ($W{\cdot}cm^{-2}$)	0.15	0.15	0.15
Pulse frequency (kHz)	245	245	245
Reverse time (μs)	1.8	1.8	1.8
Deposition procedure			
	TiAlN	AlN	TiN
Working pressure (Pa)	≈0.21	≈0.25	0.22
Table speed (RPM)	1	10	1
Satellite speed (RPM)	5	–	5
Al Power density ($W{\cdot}cm^{-2}$)	≈3	≈6 (x2)	–
Ti Power density ($W{\cdot}cm^{-2}$)	≈4	–	≈5
Substrate bias (V)	−40	−60	–
Bias pulse frequency (kHz)	250	250	–
Bias reverse time (μs)	0.5	0.5	–
Deposition time (min)	60	60	20
Target-substrate distance (mm)	100	150	100
Substrate temperature (°C)	≈180	≈200	≈100

procedure adopted closely resembles the xurography method [16].

Sapphire, Si (111), and tungsten carbide substrates (WC–Co, cutting tool ISO SPGN120308) underwent a cleaning process in ultrasonic baths, including sequential immersions in ultrasonic baths of acetone, alcohol, and distilled water for 10 min each. Subsequently, the samples were dried using compressed air, followed by compressed N_2. Due to the inclusion of the vacuum interruption steps, additional precautions were taken. Outside the vacuum chamber, following each deposition, the masking material was removed from the substrate and then cleaned with a soft cloth mildly soaked in acetone to eliminate residual glue from the Kapton® tape. The substrates were then cleaned in an ultrasonic bath of alcohol followed by distilled water for 5 min each. Lastly, the substrates were dried using compressed air and nitrogen. After cleaning, the corresponding mask was positioned on the substrate's surface. Then, the substrates were placed in the substrate holder and inserted into the vacuum chamber. An initial heating step-by-step procedure up to 100 °C was conducted inside the vacuum chamber until the ultimate vacuum was reached. The goal was to facilitate the surface degassing of residual adsorbed water. After 10 min at 100 °C, the heater was switched off, allowing to proceed with the physical etching of the surface. The etching conditions were carefully selected to activate the surface without damaging it. The time and bias voltage were considerably reduced, as depicted in Table 1, for the TiAlN (sensor and wear-resistant) and for TiN. Similar etching conditions were used for the deposition of AlN over the sensor film.

2.2. Characterization of the TiAlN temperature sensor

The TiAlN sensor's electrical resistance response to temperature, deposited in sapphire substrates, was evaluated up to 750 °C using the four-point measurement (4PM) method under vacuum to prevent surface oxidation. The 4PM analysis was performed using a four-point probe Ossila instrument conceived to measure the sheet resistance within a range spanning from 100 $m\Omega{\cdot}sq^{-1}$ to 10 $M\Omega{\cdot}sq^{-1}$. The instrument was connected to a temperature bench with four tungsten probe tips coated with gold. The heating was provided by a high-speed SiC heater PID (proportional – integral – derivative) controlled and installed in the temperature bench. The temperature bench was equipped with two calibrated thermocouples; one to regulate the SiC heater, ensuring precise temperature control, while the other served for measuring the reference temperature. The Ossila Sheet Resistance V2.0.7.1 software automatically applied the correction factors accounting for the sample geometric parameters [17]. The tungsten tips were positioned to comply with the 1.23 mm probe pitch of the instrument, and the measurements were taken with 50 °C temperature increments upon reaching the maximum temperature of 750 °C. The sheet resistance was measured only during the heating-up sequence of the tests. The three experiments were conducted without changing the setup, and the cooling procedure used was a spontaneous one (the heating system was shut down).

The electrical resistance variation of TiAlN with temperature was also analyzed using the two-point measurement (2PM) method in a vacuum environment. A high-resolution multimeter continuously monitored the electrical resistance signal with an acquisition rate of 10 samples per second. The TiAlN was deposited onto a sapphire substrate according to the mask design and utilized as reference against the TiAlN integrated into the multilayer system (referred also as sensor coating). A TiN film was deposited to form the electrical contacts. To determine the signal stabilization of the sensor, a series of temperature steps were conducted involving heating and cooling cycles between room temperature and 500 °C, while the electrical resistance was recorded. This approach allowed pinpointing the stabilization temperature at which the material's resistance reached a consistent value. Finally, a test where the sensor was heated up to 400 °C confirmed its stability. In these experiments, the heating rate was around 40 $°C.min^{-1}$. The thermal index β or thermistor sensitivity, and the TCR were calculated over the temperature range of 50–200 °C. To compute the sensitivity, the following equation was used:

$$\beta_{[50-200C]} = \frac{\ln\left(\frac{R_{T1}}{R_{T2}}\right)}{\left(\frac{1}{T_1} - \frac{1}{T_2}\right)} \quad (1)$$

In equation (1), β is in K, and R_{T1} and R_{T2} are the respective sheet resistances at temperatures T_1 and T_2. TCR was calculated within the same temperature range as the sensitivity, according to equation (2):

$$TCR = \frac{R_2 - R_1}{R_1(T_2 - T_1)} \quad (2)$$

where TCR is expressed in K^{-1} units.

The chemical composition and morphology were analyzed by field-emission scanning electron microscopy (FE-SEM) by using a ZEISS Merlin® instrument, equipped with energy-dispersive X-ray spectroscopy (EDX) technique from Oxford Instruments. The crystal structure of the compound was assessed by X-ray diffraction technique in a Panalytical X'pert equipment featuring a Co Kα radiation (λ = 0.178897 nm) source in conventional Bragg-Brentano geometry, from 30 to 80° (2θ). The analysis was performed in the as-deposited sample, and a baseline correction was applied to the XRD pattern. The peaks were fitted using a Pseudo-Voigt function to calculate the peak position (2θ) and the full width at half maximum (FWHM). Joint Committee on Powder Diffraction Standards (JCPDS) cards were used for peak identification: TiN 087–0628; AlN 46–1200. The interplanar spacing d_{hkl}-spacing was calculated using Bragg's law formula.

2.3. Characterization of the sensor coating for temperature measurement

The micro and nanostructure, morphology and elemental composition of the multilayer stack were analyzed by electron microscopy techniques. The cross-sectional analysis of the multilayer system deposited onto the cutting tool was conducted in a FEI Titan Themis Cubed microscope operated at 200 kV equipped with a Super-X system for EDX analysis. Previously, a lamella (5 μm x 4 μm x 0.1 μm – Length x Depth x Thickness) of the sample was prepared by using a Dual Beam FIB-SEM FEI Helios NanoLab 450S equipment, which combines a SEM with a Focused Ion Beam, in order to have an electron-transparent specimen (≤100 nm thickness) to be analyzed by Scanning Transmission Electron Microscopy (STEM) and EDX.

The electrical resistance variation of the sensor coating to temperature was evaluated using the same apparatus mentioned above for the 2PM method. The signal stabilization followed the same procedure for the sensor layer deposited in the sapphire substrate. Four temperature evaluation cycles (heating-cooling) between ambient temperature and 400 °C were performed to calibrate sensor coating, and the fit was done using the equation one and R25 value. The heating steps used were of 20 °C·min^{-1}, whereas the cooling was performed naturally (heating system was shut down). The calibration was executed under vacuum to prevent surface oxidation of TiN and substrate. After the calibration, the sensor coating was tested for temperatures of 200 °C. For that purpose, an Arduino® board Nano 33 IoT was used for acquiring the signals. An operational amplifier (Op Amp) – Microchip® Rail-to-Rail Input/Output MCP6042 – in conjunction with a 10 kΩ variable resistor were used for signal amplification and setpoint tuning. The temperature was maintained at 200 °C for 10 min to assess the accuracy of the complete system.

3. Results and discussion

3.1. TiAlN sensor electrical characterization four-point method

Fig. 2 (a) shows the variation of the sheet resistance with temperature variations (R-T), for three successive runs up to 750 °C, whereas Fig. 2 (b) and (c) show the schematic of the apparatus and an image of the apparatus at elevated temperatures, respectively. The observed behavior of electrical resistance is typical for a semiconductor material, as it shows a decrease in resistance with an increase in temperature [18]. After each run, the R25 reveals variability, suggesting the need to stabilize the electrical signal. The film's sensitivity diminishes from 594 to 76 K, accompanied by a corresponding decrease in the TCR value from -2.95×10^{-3} to -4.81×10^{-4} K^{-1}(the negative sign shows the tendency of the resistance). Simultaneously, the resistivity falls from 2.1×10^4 to 6.0×10^3 μΩ cm. Since at the third run, the R25 closely resembles the previous run, it indicates that after the signal stabilization, the sensitivity tends to decrease. The electrical properties of the first run are within the values reported by Martins et al. [15] for similar chemical compositions. However, the compound developed in this study reveals lower resistivity. The direct comparison is challenging since the authors did not delve into the stabilization of the signals in their work. The observed TCR, lower than documented for traditional oxide thermistors, aligns closely with conventional platinum resistance temperature detectors (RTDs) [9].

In the work by Fujita et al. [19], authors state that materials with β below 1000 K pose challenges for thermistor applications; yet, the same authors acknowledge the necessity for low β values to be able to measure broader temperature ranges [20]. While sensitivity is advantageous in capturing subtle temperature changes, obtaining reliable readings at

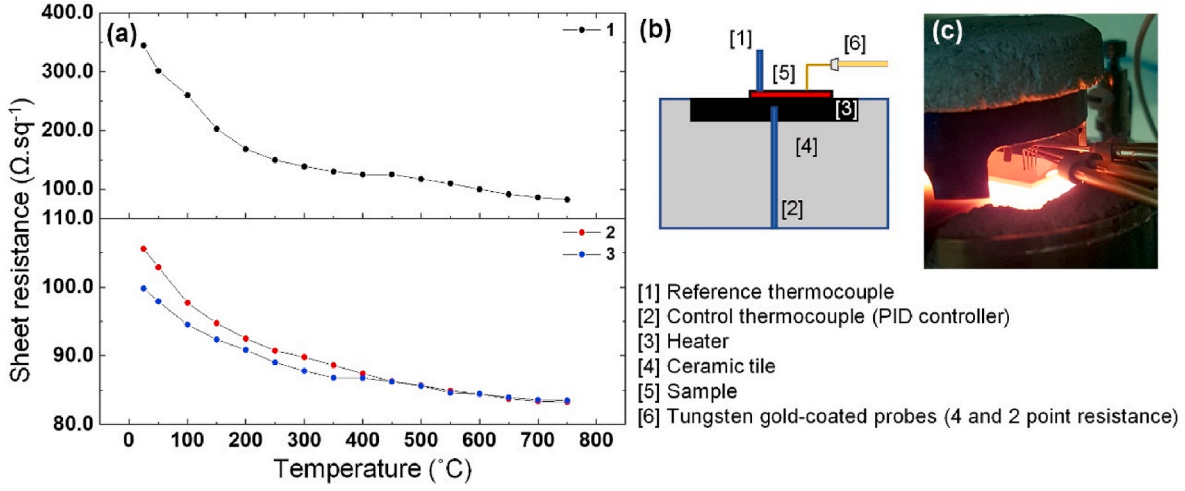

Fig. 2. (a) Sheet resistance response to temperature (up to 750 °C) with three successive runs; (b) schematic description of the experimental apparatus to retrieve the electrical signal with temperature variation; (c) image capturing the experimental setup at elevated temperatures.

high temperatures becomes challenging due to the exponential decay of resistance. In addition, the high sensitivities often come together with high resistivities [21], which adds additional complexity to electronics design for handling low-bias currents. For instance, TiAlN films with β close to 3000 K exhibited resistivities around 1.0×10^{9} μΩ cm [19].

3.2. TiAlN sensor layer structural and chemical analysis

The TiAlN single layer deposited on the sapphire substrate was analyzed by SEM-EDX before the sheet resistance experiments. The chemical composition returned a result in close agreement with the previous study [15], for Al/(Al+Ti) ratio ~ 0.56. The chemical elements content, including the light elements coming from surface contamination and Si from the substrate are presented in Table 2.

The structural analysis of the as-deposited TiAlN sensor layer is presented in Fig. 3. The film exhibits a highly textured cubic B1–NaCl crystal structure with a (111) dominant orientation at 43.73° and a weak diffraction of the (200) plane at 50.90°. Additional diffraction peaks were not detected from 30 to 40° and 55 to 80°. A similar chemical composition of Al/(Ti+Al) ratio has been found elsewhere [15,22] with similar 2θ positions. The prominent peak is situated between the standard positions of the (111) TiN and (111) AlN cubic crystal phases. The peak shifting to higher angles regarding the (111) TiN position can be explained by the substitution of the Ti atoms for the smaller Al atoms in the TiN crystal structure [23,24]. The weak phase (200) shows a similar shift. As expected, the interplanar spacing d_{hkl} computed for the plane (111) decreased from the standard 0.245 nm (interplanar spacing for TiN according to the standard position provided in the reference card) to 0.241 nm. The crystal structure of AlN is shown in Fig. A1 of the supplementary material.

3.3. TiAlN sensor layer signal stabilization

The electrical resistance changes of the TiAlN temperature sensor layer under varying cycling temperatures is presented in Fig. 4 (a). The sensor layer was deposited on a sapphire substrate with a meander design (Fig. 4 (b)) and subjected to temperatures ranging from room temperature to 500 °C within a vacuum environment. The meander design was thought to increase the film's length and the R25 value [21]. Each intermediate temperature step was held for approximately 10 min. As the temperature increases, the sensor's resistance decreases as expected, following the semiconductor's negative temperature coefficient of resistance (TCR) characteristic. However, upon closer examination, during the holding steps, and after each temperature rise, the resistance signal does not stabilize and increases by about 90 Ω. Ferreira et al. [9,25] have reported the need to stabilize their resistive film sensors. They demonstrated that signal stabilization could be achieved through thermal treatment at low temperatures and mentioned several factors that can contribute to the stabilization, such as grain refinement or grain growth and recrystallization. In this case, the resistance increase is attributed to the buildup of stresses in the TiAlN film as it undergoes thermal expansion and contraction. When the temperature decreases, the resistance value stabilizes due to structural relaxation, i.e., the film's microstructure gradually adjusts to accommodate substrate contraction. The variation in the electrical properties due to structural relaxation was also experimented by Kearney and colleagues [26], where a variation of the electrical properties of TiN films was observed. Since ΔΩ is roughly 300 Ω, which can lead to significant errors in temperature readings, post-deposition annealing was employed to promote structural relaxation and stabilization of the resistance values.

Table 2
Chemical composition for TiAlN temperature sensor layer as-deposited, given Al/(Ti+Al) ratio ~ 0.53, taken at 10 KeV.

Ti (at%)	Al (at%)	N (at%)	Si (at%)	C (at%)	O (at%)
17.7 ± 0.4	19.8 ± 0.2	56.0 ± 0.3	0.8 ± 0.1	3.3 ± 0.2	2.5 ± 0.1

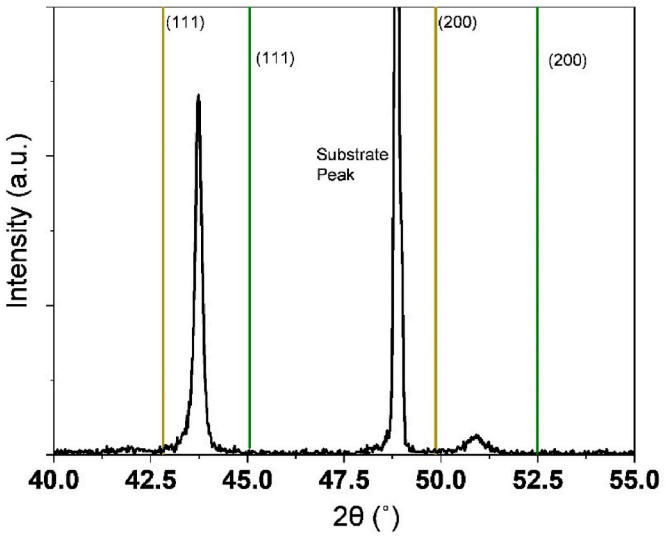

Fig. 3. TiAlN sensor XRD pattern in an as-deposited state. The standard planes displayed are assigned to AlN (111) (200) and TiN (111) (200). ICDD card numbers considered: TiN 87–0633 (pale yellow), AlN 46–1200 (green).

Fig. 5 (a) shows the resistance changes during temperature applied cycles between 300 and 400 °C. Here, the resistance exhibits a significant improvement regarding stability, after being subjected around 15 min at 300 and 400 °C, as evidenced by the decrease in the resistance change (ΔΩ) of approximately 10 Ω (0.5% full range) after temperature cycling. This outcome suggests that a thermal treatment at these conditions allows the film to fully relax and eliminate any residual stresses that could affect its electrical properties, which is completely feasible in situ in modern PVD equipment (possible to heat the substrates up to 600 °C). Fig. 5 (b) shows the R-T experiment results after signal stabilization, highlighting the absence of hysteresis within the heating and cooling curves. The sensitivity and TCR values calculated were about 65 K and $-4.1\times10^{-4}\,K^{-1}$, respectively, in coherence with what is observed in Fig. 2. As mentioned before, the sensitivity of the nitride film is far from what is observed in the conventional thermistor sensors; however, low sensitivity means that the material has an almost linear resistance response to temperature variations. A recent study shows a growing demand for linear thermistors to reduce instrumentation complexity, where our material presents a promising solution [27].

3.4. Chemical, morphological, and electrical characterization of sensor coating

After validating the usage of the TiAlN layer as a temperature sensor, hereafter, the characterization of the TiAlN film embedded in a multilayer system, which is termed sensor coating, was performed. Fig. 6 provides a HAADF-STEM cross-sectional view of the multilayer architecture deposited over the cutting tool, revealing the columnar morphology of the coating. The complete stack image, including the Zr adhesion interlayer, is presented in the supplementary material as Fig. A2. The spatial distribution of the main elements (Ti, Al, and N) throughout the coating thickness is also displayed. The presence of a droplet (marked as 1 in Fig. 6) and voids (marked as 2 in Fig. 6) can be observed. Based on the elemental map, the droplet is identified as Ti-rich, suggesting its formation from arcing events during the deposition of AlN. The low bias applied to the substrate and the absence of heating during the deposition likely contributed to the reduced mobility of adatoms, i.e., low kinetic energy, hindering the formation of dense columns. Iqbal and Yasin [28] elaborated on the relevancy of the deposition conditions to form AlN thin films by reactive sputtering

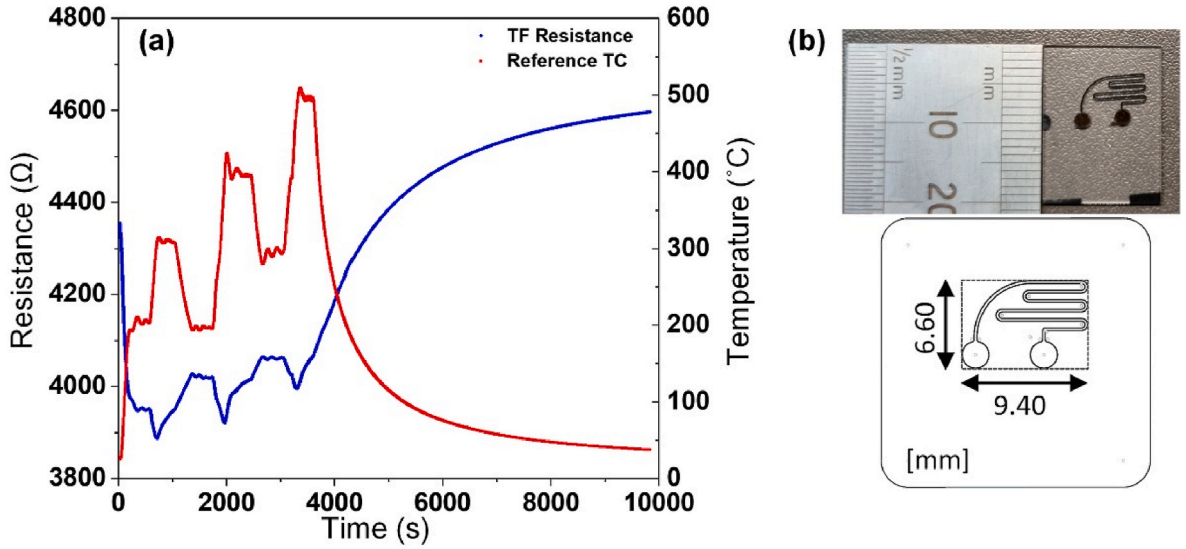

Fig. 4. (a) Electrical resistance response of the TiAlN sensor, under varying cycling temperatures, reaching a maximum of 500 °C within a vacuum environment and deposited in a meander pattern. (b) A meander pattern was designed for the TiAlN sensor deposited in the sapphire substrate and respective overall dimensions.

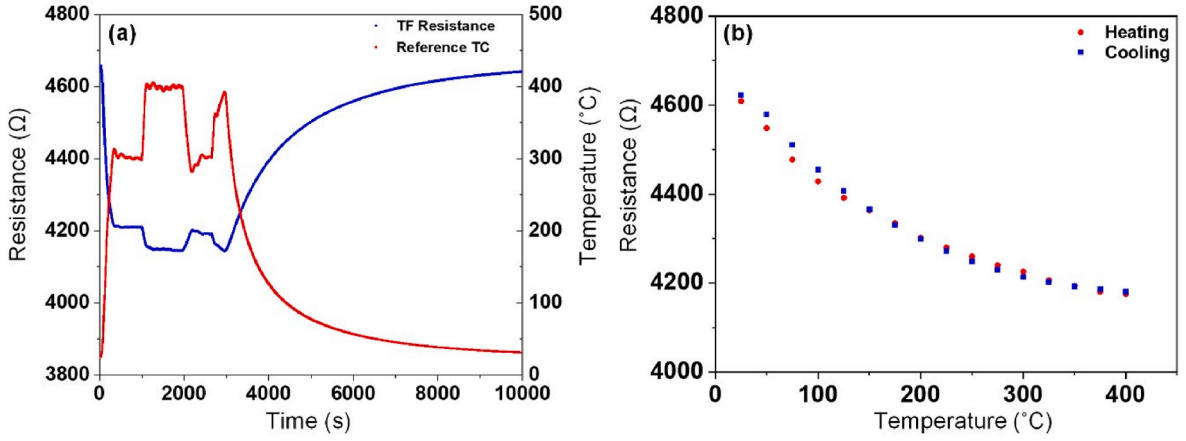

Fig. 5. (a) Signal stabilization experiment performed under vacuum; temperature cycling range between 300 and 400 °C. (b) R-T test after stabilization performed under vacuum up to 400 °C.

processes, which can be used as a general guide for optimizing nitride deposition. The intermediate ion etching steps performed between vacuum interruptions were beneficial for promoting good interlocking between the different layers. However, they were insufficient to completely disrupt the extension of the columns and the presence of voids between them. Above the Ti-rich droplet, the Ti thin adhesion layer is clearly observable, followed by the wear-resistant layer that transitions into TiAlN through a controlled gradient, as detailed in the experimental methods section.

Further optimization of the deposition process may help minimize void formation and improve the overall microstructure of the multilayer coating. Nevertheless, protecting the underlying layers must always be considered when developing a new one, which was accomplished in this study. Independently of the waviness aspect of the multilayer layers a continuation growth of the columns can be observed. Changes in the microstructure, such as voids and cracks, may disrupt film's continuity causing electrical resistance and signal variations. These defects can act as scattering centers, hindering the efficient transport of charge carriers [29]. The presence of voids, with a significantly higher number than the one of the droplets, implies that their role in the overall resistance is more pronounced and may lead to the electrical failure of the system. For instance, some of the prepared samples did not function as sensors by exhibiting low electrical resistance (~10 Ω).

A detailed view of the embedded TiAlN sensor and its interface arrangement with AlN is presented in Fig. 7. Upon a closer examination of the sensor layers, it is possible to discern a clear multilayer structure, a feature not readily apparent in Fig. 6. The layers exhibit alternating light and dark contrasts, including thin sublayers, on the order of a few nanometers. This thinness is attributed to the simultaneous sputtering of Ti and Al from four targets, coupled with the movement of the substrates within the deposition chamber. The alternating light and dark bands in the TiAlN sensor correspond to Al-poor and Al-rich zones, as depicted in the EDXS maps presented in Fig. 8, suggesting a controlled growth process. The two-fold rotation mode, widely employed in the industry for cutting tools and replicated in this study, plays a crucial role in achieving uniform coatings over complex shapes [30]. However, substrates travel through different plasma zones, leading to intricate multilayer systems like the one presented in this study.

The TiAlN multilayer layer exhibits a columnar morphology, with well-defined columns perpendicular to the AlN layer. The columnar morphology is attributed to the shadowing effect of the incoming atomic flux, which causes the adatoms to be deposit preferentially on the top of the growing columns. The limited adatom mobility contributes to the formation of sharp columnar boundaries and to the creation of voids or

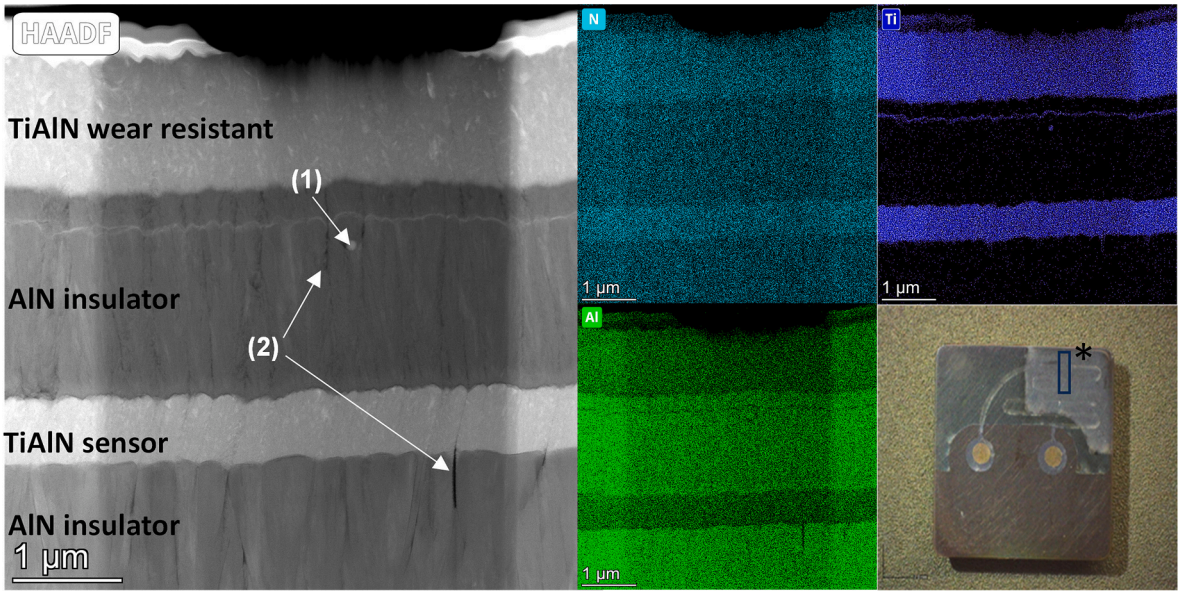

Fig. 6. High-Angle Annular Dark-Field STEM images of the multilayer stack coating deposited on WC-Co substrate, showing the presence of some growth defects (labels 1 and 2). EDX spectroscopy maps show the elemental distribution of Al, Ti, and N along the thickness. The FIB cut (lamella) was performed in the area depicted with * in the top view of the cutting tool.

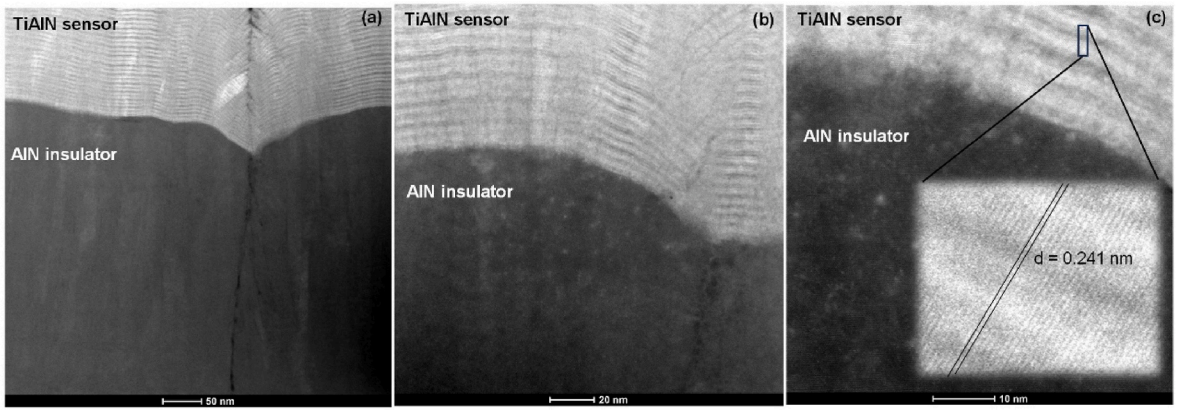

Fig. 7. High-Angle Annular Dark-Field STEM images of the sensor layer TiAlN and the interface with AlN deposited on W/C–Co substrate, from lower to higher magnification (a–c). (c) The inset shows the orientation of the (111) planes and interplanar distance.

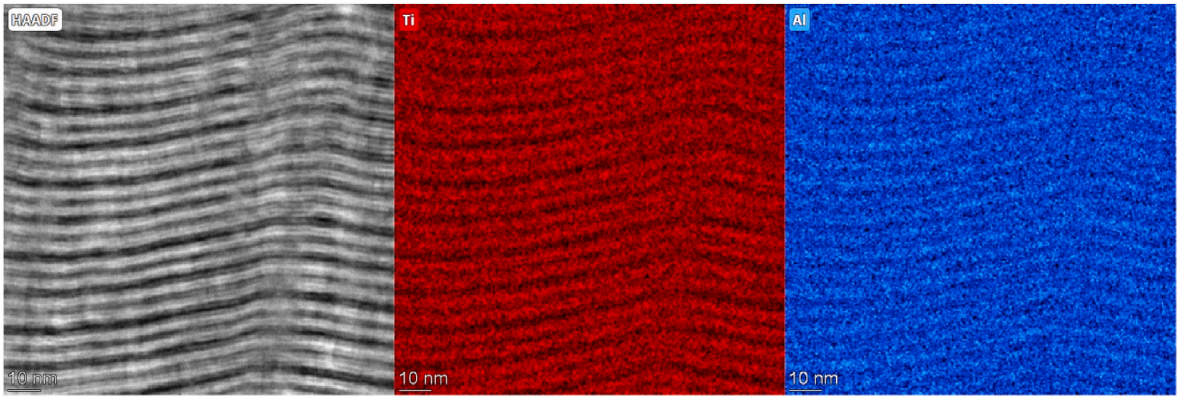

Fig. 8. Detailed High-Angle Annular Dark-Field STEM image of the sensor layer TiAlN with the respective EDX Spectroscopy maps. EDXS maps show the elemental spatial distribution of Al and Ti elements.

to the separation between the columns, which is detected in Fig. 7 (a) and (b). During the R-T experiments, the elongation of the film could amplify the spaces between the columns, compromising the conductivity of the sample. During the cooling phase, the relaxation of the film may reduce the space between columns, stabilizing the electrical signal. This process is assumed to occur for signal stabilization during the thermal experiments. The interface between the TiAlN and AlN layer is sharp, but the nanolayered structure of TiAlN has diffuse interfaces; that are not considered as superlattices (Fig. 7 (c)). Additional defects are detected in the sensor layer, where a stacking fault is distinguished due to the void formation between the AlN columns. Before the deposition of the TiAlN sensor layer, the intermediate ion etching step did not cause any microstructural alteration to the AlN layer, suggesting that the process was well controlled. Additionally, in the inset of Fig. 7 (c), the magnification of the multilayered plane (not to scale), which covers the thickness, suggests the same preferred orientation with an interplanar spacing close to 0.241 nm [31], showing a total coherency across all the interfaces. This agrees well with the XRD information and supports the classification of the Ti(Al)N as a fcc solid solution alternating with Al-rich/poor zones.

3.5. Sensor coating electrical characterization and temperature sensor functionality

The validation of the sensor coating usage for temperature readings was addressed in this study using a popular developer platform for electronics – Arduino board. Signal stabilization was first performed to assess the sensor coating. The multilayer coating was submitted to 400 °C for 20 min, while a multimeter was used to monitor the electrical resistance. Fig. 8 (a) depicts the experiment, where it is possible to observe the increase in the resistance when maximum temperature is reached again. The cutting tool was allowed to rest in place until the signal started to dampen, which started around 20 min after the beginning of the experiment. As mentioned in the experimental methods section, this test was performed under vacuum to avoid oxidation of the TiN contacts and the substrate. We understand that these temperatures (above 400 °C) can promote surface oxidation and affect the sensor readings. As the TiAlN sensor is protected by AlN and TiAlN outer layers, oxidation of the sensor layer is not expected in an atmospheric environment. In addition, in metal-cutting applications, TiN is positioned far from high-temperature locations where the tool and workpiece come into contact; therefore, it is not susceptible to oxidation in usual use cases [8,11,32].

Fig. 8 (b) shows the outcome of the four heating-cooling cycles for which the average and standard deviation were computed after stabilization. The sensitivity was higher than reported for the single layer; however, it is known that different substrates originate different electrical properties [33]. The fit was performed using the equation displayed in Fig. 8 (b) since utilizing the Beta value simplifies the calibration method, at the expense of slightly increasing the measurement error. The fit stays well within the average and standard deviation found for the sensor coating. The multilayer coating exhibited good sensitivity and stability, indicating its potential for temperature measurement applications up to 400 °C.

Nevertheless, the difference in the R25 value must be considered for future measurements with additional samples coming from different deposition batches. This is not of concern if the beta value is more or less stable throughout different depositions; however, if it changes considerably, all the coatings must be calibrated, which is unfeasible. This variability could be attributed to the reduction in the breakdown voltage after the deposition of the TiN contact over the sensor. As a consequence of the found voids in the cross-sectional view of the multilayer system, some may act as short-circuit paths after the inclusion of the conductive TiN, which substantially reduces the resistance. In addition, when the samples are subjected to temperature, these defects can cause inconsistent behavior in the TiAlN sensor (Figure A3 in the supplementary material provides an example). Despite these limitations, it was possible to use the tool as intended, exhibiting good stability and making it suitable for various applications, like high-stress environments such as metal cutting or high-speed machining, where significant temperature variations are expected.

Due to the minor sensitivity of ~100 K presented by this coating; amplification of the signal was implemented since the resolution of the Arduino board used is only of 12-bit. With the proper amplification, it was possible to increase the resolution (~10 times) of the system from a 0.1 °C/ADC resolution to 0.01 °C/ADC one. Fig. 10 illustrates the signal acquisition system designed for this application and the respective error associated with the instrumentation. The variable resistor is used to tune the signal for room temperature, acting also as the reference resistor for the voltage divider. In Fig. 10 (a), it is possible to recognize, in the first seconds of the experiment, some noise derived from the knob adjustment of the variable resistor for tuning the room temperature. The test runs up to 200 °C to compute the error and confirm its functionality as a temperature sensor. Fig. 9 (a) insets shows in the cutting tool with the sensor coating and with the measurement probes connected to the TiN contacts. Fig. 10 (b) illustrates two OpAmps since the thinkers Tinkercad® program used in this study does not have the OpAmp specified in the methods section; in reality, only one is used. By using a board with Wi-Fi connectivity, it is possible to use these sensors for remote applications without the need for wiring. The error computed for the sensor coating is around 6%, which is less than the error obtained in Lian et al. work [10] regarding the TFTCs developed to measure the temperature during the cutting of titanium.

4. Conclusion

This study successfully integrated a TiAlN temperature sensor within a multilayered system considered for harsh applications, particularly metal cutting. The single layer exhibited semiconductor behavior up to 750 °C and proved stable for temperature measurement applications integrated as a coating stack, validated up to 400 °C. While the potential for higher temperatures is acknowledged, further testing involving all layers is essential for exhaustive validation. The cross-section examined by STEM revealed the columnar morphology of the sensor coating, containing typical PVD growth defects such as voids and droplets. Notably, these defects did not compromise the stability of the multilayer, although there may be implications regarding undesirable short-circuit situations. In addition, the intermediate conditions considered between the vacuum interruptions for masking procedures, including ion energy and temperature, proved effective in ensuring interlocking between the various layers.

Despite the higher Al content, the TiAlN temperature sensor exhibits a cubic crystal structure defined by diffuse nanolayers – alternating in Al content – resulting from the selected two-fold rotational movement. The columnar morphology, a consequence of the shadowing effect during deposition, presented challenges such as voids and separation between columns. Nevertheless, the sensor coating exhibited promising stability and reproducibility for temperature measurements up to 400 °C. The signal acquisition system, comprising a variable resistor and an OpAmp, effectively addressed the variability in the R25 and low sensitivity values, yielding a measurement error of approximately 6%. In addition, the approach presents a solution for remote measurements with implications across various industrial sectors. As future research, this study lays the groundwork for extending the system's capabilities by exploring temperature measurements during the cutting of titanium alloy.

CRediT authorship contribution statement

Bruno Martins: Investigation, Visualization, Writing – original draft. **Carlos Patacas:** Investigation, Visualization. **Albano Cavaleiro:** Conceptualization, Supervision, Validation, Writing – review & editing. **Pedro Faia:** Investigation, Writing – review & editing. **Fátima Zorro:**

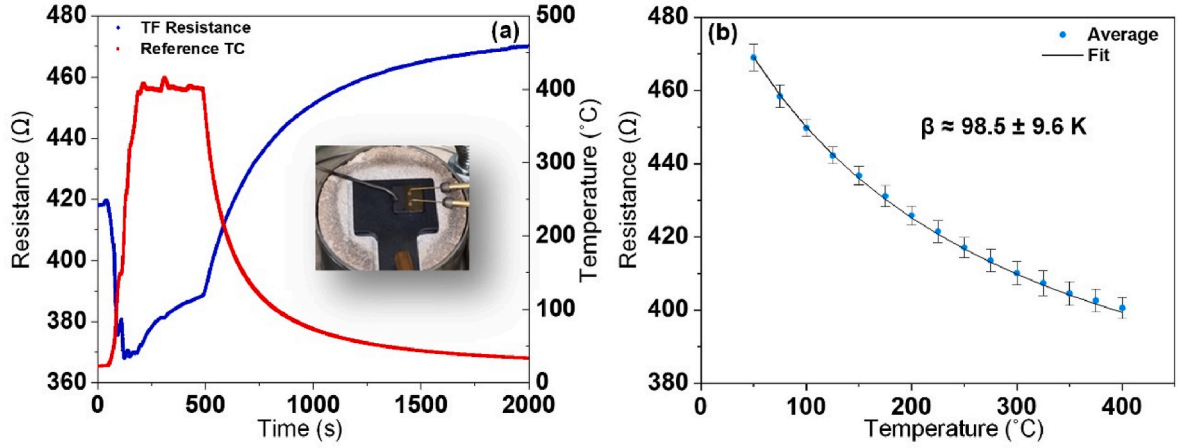

Fig. 9. (a) Electrical response to temperature at 400 °C for 20 min in a vacuum atmosphere. The inset in the figure shows the apparatus for the 2PM method (b) R-T experiments up to 400 °C after signal stabilization.

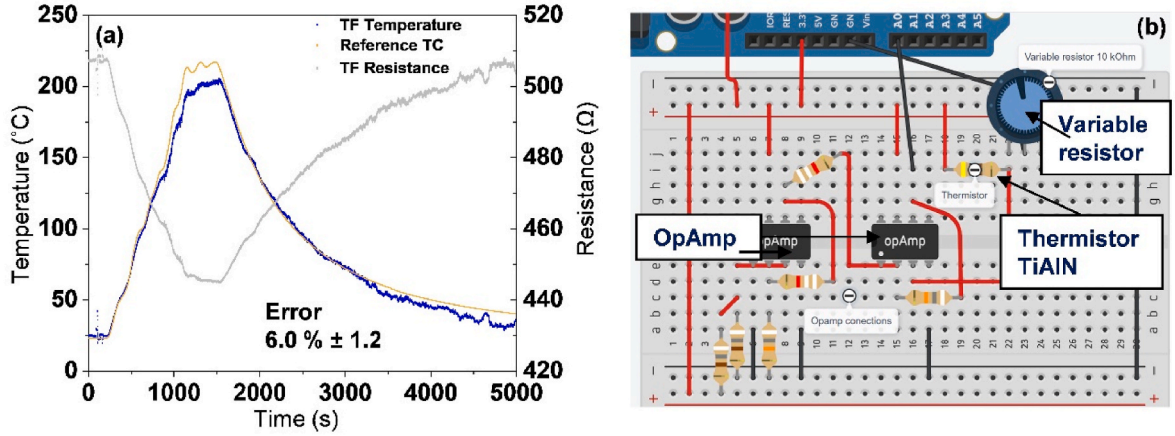

Fig. 10. (a) Determination of the error associated with the complete temperature measurement system. The blue line corresponds to the temperature reading with the Arduino® board, and the orange line with the temperature readings by the reference thermocouple – the grey line corresponds to the resistance reads, also with the Arduino®; (b) Tinkercad® schematic to simulate the apparatus with the respective components in a breadboard and the Arduino® port connections – similar to Arduino® board Nano 33 IoT used in this study.

Investigation. **Enrique Carbo-Argibay:** Investigation, Writing – review & editing. **Paulo J. Ferreira:** Investigation. **Filipe Fernandes:** Conceptualization, Supervision, Validation, Writing – review & editing.

Declaration of competing interest

The authors declare that they have no known competing financial interests or personal relationships that could have appeared to influence the work reported in this paper.

Acknowledgements

The authors would like to extend a special thanks to Dr. Cristiana Alves, the INL facility manager, for promptly performing an EDX spectroscopy analysis on the TiAlN sensor layer.

This research is sponsored by national funds: Soft4Sense project "Smart Surfaces for Reliable Tooling Integration" (reference: POCI-01-0247-FEDER-045921), co-financed by the European Regional Development Fund, through Portugal 2020 (PT2020), by the Competitiveness and Internationalization Operational Programme (COMPETE 2020) and Foundation for Science and Technology (FCT) is also acknowledged. This research is also sponsored by national funds through FCT, under projects UIDB/00285/2020, LA/P/0112/2020 and LAETA Base Funding (DOI: 10.54499/UIDB/50022/2020).

Appendix A. Supplementary data

Supplementary data to this article can be found online at https://doi.org/10.1016/j.jsamd.2024.100716.

References

[1] S. Bagavathiappan, B.B. Lahiri, T. Saravanan, J. Philip, T. Jayakumar, Infrared thermography for condition monitoring - a review, Infrared Phys. Technol. 60 (2013) 35–55, https://doi.org/10.1016/j.infrared.2013.03.006.

[2] M. Moreno, J.M. Andersson, R. Boyd, M.P. Johansson-Jöesaar, L.J.S. Johnson, M. Odén, L. Rogström, Crater wear mechanism of TiAlN coatings during high-speed metal turning, Wear (2021) 484–485, https://doi.org/10.1016/j.wear.2021.204016.

[3] M. Danek, F. Fernandes, A. Cavaleiro, T. Polcar, Influence of Cr additions on the structure and oxidation resistance of multilayered TiAlCrN films, Surf. Coating. Technol. 313 (2017) 158–167, https://doi.org/10.1016/j.surfcoat.2017.01.053.

[4] Y. Niu, H. Dong, H. Wang, T. Liu, X. Li, Q. Tan, J. Xiong, Design and performance evaluation of an all-ceramic high-temperature test sensor, J. Alloys Compd. 938 (2023) 168561, https://doi.org/10.1016/j.jallcom.2022.168561.

[5] K. Bobzin, T. Brögelmann, N.C. Kruppe, J. Janowitz, Smart PVD hard coatings with temperature sensor function, Surf. Coating. Technol. 423 (2021), https://doi.org/10.1016/j.surfcoat.2021.127631.

[6] S. Biehl, E. Meyer-Kornblum, N. Paetsch, G. Bräuer, Novel sensor modules for efficient manufacturing of natural fiber reinforced plastics, Proceedings 2 (2018) 918, https://doi.org/10.3390/proceedings2130918.

[7] S. Biehl, N. Paetsch, E. Meyer-Kornblum, Thin film system with integrated load and temperature sensors for the technical application in deep drawing process, Smart Sensors, Actuators, MEMS VIII. 10246 (2017) 102460O, https://doi.org/10.1117/12.2265694.
[8] T. Li, T. Shi, Z. Tang, G. Liao, J. Han, J. Duan, Temperature monitoring of the tool-chip interface for PCBN tools using built-in thin-film thermocouples in turning of titanium alloy, J. Mater. Process. Technol. 275 (2020) 116376, https://doi.org/10.1016/j.jmatprotec.2019.116376.
[9] E. Oliveira, J.P. Silva, J. Laranjeira, F. Macedo, S. Lanceros-Mendez, F. Vaz, A. Ferreira, Fabrication, characterization and implementation of thermo resistive ticu(N, O) thin films in a polymer injection mold, Materials 13 (2020), https://doi.org/10.3390/ma13061423.
[10] Y. Lian, X. Chen, T. Zhang, C. Liu, L. Lin, F. Lin, Y. Li, Y. Chen, M. Zhang, W. Zhou, Temperature measurement performance of thin-film thermocouple cutting tool in turning titanium alloy, Ceram. Int. 49 (2023) 2250–2261, https://doi.org/10.1016/j.ceramint.2022.09.193.
[11] T. Li, T. Shi, Z. Tang, G. Liao, J. Duan, J. Han, Z. He, Real-time tool wear monitoring using thin-film thermocouple, J. Mater. Process. Technol. 288 (2021) 116901, https://doi.org/10.1016/j.jmatprotec.2020.116901.
[12] P.R.N. Childs, J.R. Greenwood, C.A. Long, Review of temperature measurement, Rev. Sci. Instrum. 71 (2000) 2959–2978, https://doi.org/10.1063/1.1305516.
[13] C. Wang, G.Y. Hong, K.M. Li, H.T. Young, A miniaturized nickel oxide thermistor via aerosol jet technology, Sensors 17 (2017), https://doi.org/10.3390/s17112602.
[14] S. Suzuki, T. Fujita, Y. Hosokawa, K. Fujiwara, N. Nagatomo, Development of a wurtzite (Al,Ti)N thermistor on a resin substrate with high heat resistance, J. Ceram. Soc. Japan. 129 (2021) 355–358, https://doi.org/10.2109/jcersj2.20224.
[15] B. Martins, C. Patacas, A. Cavaleiro, P. Faia, O. Bondarchuk, F. Fernandes, Electrical properties and thermistor behavior of TiAlN thin films deposited by combinatorial sputtering, Surf. Coat. Technol. 464 (2023) 129545, https://doi.org/10.1016/j.surfcoat.2023.129545.
[16] D.A. Bartholomeusz, R.W. Boutté, J.D. Andrade, Xurography: rapid prototyping of microstructures using a cutting plotter, J. Microelectromech. Syst. 14 (2005) 1364–1374, https://doi.org/10.1109/JMEMS.2005.859087.
[17] I. Miccoli, F. Edler, H. Pfnür, C. Tegenkamp, The 100th anniversary of the four-point probe technique: the role of probe geometries in isotropic and anisotropic systems, J. Phys. Condens. Matter 27 (2015) 223201, https://doi.org/10.1088/0953-8984/27/22/223201.
[18] T. Dinh, H.P. Phan, A. Qamar, P. Woodfield, N.T. Nguyen, D.V. Dao, Thermoresistive effect for advanced thermal sensors: fundamentals, design considerations, and applications, J. Microelectromech. Syst. 26 (2017) 966–986, https://doi.org/10.1109/JMEMS.2017.2710354.
[19] T. Fujita, H. Tanaka, H. Inaba, N. Nagatomo, Development and electrical properties of wurtzite (Al,Ti)N materials for thin film thermistors, J. Ceram. Soc. Japan. 124 (2016) 653–658, https://doi.org/10.2109/jcersj2.15316.
[20] T. Fujita, K. Fujiwara, T. Yamaguchi, Electrical properties of La(Cr,Mn)O3 NTC materials, Key Eng. Mater. 485 (2011) 237–240. https://doi.org/10.4028/www.scientific.net/KEM.485.237.
[21] A. Feteira, Negative temperature coefficient resistance (NTCR) ceramic thermistors: an industrial perspective, J. Am. Ceram. Soc. 92 (2009) 967–983, https://doi.org/10.1111/j.1551-2916.2009.02990.x.
[22] C. Jiménez, C. Sánchez-Fernández, C. Morant, J. Martínez-Duart, M. Fernández, J. Sánchez-Olías, Dependence of the mechanical and structural properties of (Ti , Al) N films on the nitrogen content, J. Mater. Res. 14 (1999) 7, https://doi.org/10.1557/JMR.1999.0378.
[23] F.C. Yang, C.Y. Lin, J.F. Tang, C.L. Chang, Effect of mid-frequency pulse insertion on the microstructural and mechanical properties of AlTiN coatings prepared using superimposed HiPIMS process, Surf. Coating. Technol. 388 (2020) 125597, https://doi.org/10.1016/j.surfcoat.2020.125597.
[24] S. Liu, K. Chang, S. Mráz, X. Chen, M. Hans, D. Music, D. Primetzhofer, J. M. Schneider, Modelling of metastable phase formation for sputtered Ti1-xAlxN thin films, Acta Mater. 165 (2019) 615–625, https://doi.org/10.1016/j.actamat.2018.12.004.
[25] A. Ferreira, M.A. Correa, J.P. Silva, D. Correia, S. Lanceros-Mendez, F. Vaz, Multifunctional hard coatings based on CrNx for temperature sensing applications, Sensors Actuators, A Phys. 329 (2021), https://doi.org/10.1016/j.sna.2021.112794.
[26] B.T. Kearney, B. Jugdersuren, J.C. Culbertson, P.A. Desario, X. Liu, Substrate and annealing temperature dependent electrical resistivity of sputtered titanium nitride thin films, Thin Solid Films 661 (2018) 78–83, https://doi.org/10.1016/j.tsf.2018.07.001.
[27] Z. Li, Y. Liu, R. Wu, A. Chang, B. Zhang, New linear high-temperature thermistors based on the xAl2O3-(1-x)CaMnO3 ceramics, Ceram. Int. 49 (2023) 18035–18041, https://doi.org/10.1016/j.ceramint.2023.02.171.
[28] A. Iqbal, F. Mohd-Yasin, Reactive sputtering of aluminum nitride (002) thin films for piezoelectric applications: a review, Sensors (Switzerland) 18 (2018) 1–21, https://doi.org/10.3390/s18061797.
[29] S. Pawar, K. Singh, S. Sharma, A. Pandey, S. Dutta, D. Kaur, Growth assessment and scrutinize dielectric reliability of c-axis oriented insulating AlN thin films in MIM structures for microelectronics applications, Mater. Chem. Phys. 219 (2018) 74–81, https://doi.org/10.1016/j.matchemphys.2018.08.013.
[30] M. Panjan, T. Peterman, M. Čekada, P. Panjan, Simulation of a multilayer structure in coatings prepared by magnetron sputtering, Surf. Coating. Technol. 204 (2009) 850–853, https://doi.org/10.1016/j.surfcoat.2009.08.026.
[31] N.J.M. Carvalho, E. Zoestbergen, B.J. Kooi, J.T.M. De Hosson, Stress analysis and microstructure of PVD monolayer TiN and multilayer TiN/(Ti,Al)N coatings, Thin Solid Films 429 (2003) 179–189, https://doi.org/10.1016/S0040-6090(03)00067-1.
[32] J. Li, B. Tao, S. Huang, Z. Yin, Built-in thin film thermocouples in surface textures of cemented carbide tools for cutting temperature measurement, Sensors Actuators, A Phys. 279 (2018) 663–670, https://doi.org/10.1016/j.sna.2018.07.017.
[33] I. Krylov, X. Xu, Y. Qi, K. Weinfeld, V. Korchnoy, M. Eizenberg, D. Ritter, Effect of the substrate on structure and properties of titanium nitride films grown by plasma enhanced atomic layer deposition, J. Vac. Sci. Technol. 37 (2019) 060905, https://doi.org/10.1116/1.5109717.